Dalton Transactions

ROYAL SOCIETY OF CHEMISTRY

PAPER

View Article Online
View Journal | View Issue

Cite this: *Dalton Trans.*, 2024, **53**, 12281

Disentangling the "tip-effects" enhanced antibacterial mechanism of Ag nanoparticles†

Shenli Wang,*[a] Yanping Zhang,[a] Xuan Chen,[b] Stefanos Mourdikoudis,[c] Shengshi Fan,[b] Haoyu Li,[b] Sergio Gómez-Graña,[c] Shuncheng Ren[a] and Guangchao Zheng *[b,d]

Received 20th April 2024,
Accepted 24th June 2024

DOI: 10.1039/d4dt01173b

rsc.li/dalton

Silver nanoparticles (Ag NPs) exhibit strong antibacterial activity and are widely used in industries such as medical, food and cosmetics. In this study, Ag nanospheres and Ag nanotriangles are selected as antibacterial agents to reveal the distinct mechanism of tip effects towards their antibacterial performance. A series of antibacterial experiments were implemented, including *in situ* monitoring as well as studying and determining the evolution of the inhibition zone, minimum inhibitory concentration (MIC)/minimum bactericidal concentration (MBC) values, growth kinetics, bactericidal curve, bacterial morphologies and intracellular reactive oxygen species (ROS). Ag nanotriangles can eradicate *E. coli* and *S. aureus* at extremely low concentrations in comparison to Ag nanospheres, in particular under sunlight irradiation. The destroyed bacterial cell walls were examined by scanning electron microscopy. Through the investigation of ROS production, the generation efficiency of ROS is improved by the merit of sunlight irradiation thanks to the localized surface plasmon resonance (LSPR) properties of Ag NPs. However, a more significant improvement in ROS generation efficiency occurred in the presence of Ag nanotriangles contributed by the pronounced "tip effects". This study sheds light on the structure–performance relationship for the rational design of antibacterial agents.

1. Introduction

One-third of the world's food for human consumption (about 1.3 billion tons) is wasted annually.[1] The main causes of food spoilage and deterioration are physical, chemical, enzymatic,[2] and microbial hazards.[3] Microbial contamination is a key factor in food waste and foodborne diseases.[4,5] Food waste leads to significant economic losses in the food industry. Furthermore, the occurrence of foodborne diseases is mostly caused by the consumption of contaminated food.[6] Foodborne pathogens are a major cause of human deaths, hospitalizations and illnesses. According to the statistics provided by the Center for Disease Control and Prevention (CDCP) in the United States, foodborne diseases caused by bacterial contamination alone result in 3000 deaths and 48 million illnesses.[7] Traditional antimicrobial drugs can lead to the development of resistance. Therefore, there is an urgent need for new, safe, and effective antimicrobial agents to prevent microbial contamination and ensure food safety.

The development of nanotechnology has given rise to new achievements in the field of antibacterial agents.[8–11] Nanomaterials, with their high surface area to volume ratio as well as their unique physical and chemical properties, have shown great potential for antibacterial applications.[12–14] Importantly, the key factor of drug resistance for nanomaterials against bacteria has decreased significantly. Among them, Ag-based NPs have often been reported to serve as suitable antibacterial nanomaterials due to their excellent optical and bactericidal properties. Ag NPs, as broad-spectrum antibacterial agents, have good sterilization properties and effectively inhibit the growth of bacteria, fungi and algae.[15–17] So far, several different antibacterial mechanisms have been described for silver-based NPs.[18–20] On one hand, silver ions leaching from the surfaces of Ag NPs can break the cell membranes and they are investigated for their antibacterial activity against various microorganisms. Due to electrostatic interactions, Ag^+ is adsorbed and enters the bacterial cell membrane, causing damage to it.[21] Furthermore, Ag^+ can be activated to produce reactive oxygen species (ROS) in the presence of water, achieving antibacterial effects.[22–24] On the other

[a]*College of Food Science and Technology, Henan University of Technology, Zhengzhou 450001, China. E-mail: wangshenli@163.com*
[b]*School of Physics and Laboratory of Zhongyuan Light, Zhengzhou University, Zhengzhou 450001, P. R. China. E-mail: gczheng@zzu.edu.cn*
[c]*CINBIO, Universidade de Vigo, Materials Chemistry and Physics Group, Department of Physical Chemistry, Campus Universitario Lagoas Marcosende, 36310 Vigo, Spain*
[d]*Institute of Quantum Materials and Physics, Henan Academy of Sciences, Zhengzhou 450046, China*

† Electronic supplementary information (ESI) available. See DOI: https://doi.org/10.1039/d4dt01173b

hand, the localized surface plasmon resonance (LSPR) of Ag NPs is induced by the collective oscillation of their conductive free electrons under laser irradiation, generating hot electrons and a huge electromagnetic field.[25–27] In this way, the efficiency of ROS production provoked by the newly generated hot electrons is enhanced for effective antibacterial killers.[28–31] Thus, Ag-based NPs have been regarded as a key player in the category of antibacterial agents.

As a matter of fact, the antibacterial activity and LSPR properties of Ag NPs strongly rely on their morphologies.[32–34] For instance, the differences in the particle shape lead to modifications in the surface area, surface charge and chemical interface, resulting in varying interactions with cells, cell membranes, organelles, proteins and DNA. As previously reported, rod, prism, cubic and branch-like nanostructures with more tips can help to apply a more intense electric field surrounding their tips, enabling the generation of more energetic hot electrons. From the point of view of chemistry, the tips on the nanoparticles possess a high surface energy and small curvature, easily releasing Ag^+ from the nanoparticles. The high-index facets show a relatively strong tendency to attach to the bacterial surfaces. In addition, the abundant hot electrons or electromagnetic field prefers to be localized near the tips of Ag nanotriangles, improving the ROS production. For instance, El-Zahry *et al.*[35] studied the antibacterial effects of sphere-like, triangular-like and hexagonal-like Ag NPs against *E. coli*, revealing that hexagonal-like Ag NPs exhibited stronger antibacterial activity and wound healing efficiency. In contrast, the bacterial cell wall can be physically protruded by the sharp tips of nanoparticles. The sharp tips used as "nano-needles" can damage the bacterial cell walls upon physical contact, leading to leakage of cellular components such as DNA, RNA and proteins.[36,37] All these effects on the antibacterial performance of nanoparticles are defined as "tip effects". Thus, unravelling the mechanisms of "tip effects" on the Ag antibacterial agents is of great importance in the Ag NP-based nanoscience and nanotechnology sector.

Herein, we investigated the tip effects regarding the antibacterial activity of Ag hybrid NPs against *E. coli* and *S. aureus*, employing Ag NPs with two distinct morphologies (*i.e.* spheres and triangles). Ag nanotriangles possessing sharp edges, vertices and high atomic density (111) planes allow us to explore their pronounced "tip effects". *E. coli* and *S. aureus* are treated with Ag NPs under dark conditions, permitting us to investigate the antibacterial effects of Ag ions on the tips of Ag NPs. Following this, light irradiation helped to study the antibacterial effects of Ag NPs dominated by their LSPR properties. As a result, tip effects of Ag NPs showing high surface free energy and electromagnetic field dominate the antibacterial efficiency, revealing the structure-performance relationship of the antibacterial agents.

2. Experimental

2.1 Materials

Strains: *E. coli* CMCC and *S. aureus* CMCC were obtained from China Industrial Microbial Culture Collection Management Center; Luria–Bertani (LB) Broth: Beijing Aoboxing Biotechnology Co., Ltd. AGAR powder: Tianjin Kemiou Chemical Reagent Co., Ltd. Silver nitrate ($AgNO_3$), hexadecyltrimethylammonium bromide (CTAB), sodium borohydride ($NaBH_4$), sodium citrate, hydroxylamine hydrochloride and ascorbic acid (AA) were bought from Acros. Sodium chloride, ethanol and glycerol (analytically pure) were purchased from Tianjin Tianli Chemical Reagent Co., Ltd. DI water (18.25 MΩ cm).

2.2 Methods

2.2.1 Synthesis of Ag nanospheres. The synthetic method for Ag nanospheres follows our previous report,[38] using hydroxylamine hydrochloride as the reducing agent and capping agent. First, 1.485 mL of NaOH (0.1 M) was injected into 45 ml of hydroxylamine hydrochloride (1.7 mM). Afterwards, 5 mL of $AgNO_3$ solution (10 mM) were added into the above solution. The solution was kept still for 2 hours. Spherical Ag NPs were isolated through centrifugation (8000 rpm; 10 min) and stored in water at 4 °C with a concentration of 120 μg mL^{-1}.

2.2.2 Synthesis of Ag nanotriangles. The synthesis of Ag nanotriangles was based on a seed-mediated growth approach. For seed preparation, 5 mL of $AgNO_3$ solution (20 mM) were injected into 5 mL of 0.8 mM CTAB, followed by the rapid addition of 300 μL $NaBH_4$ (10 mM) solution. After stirring for 2 min, the seed solutions were kept in the dark for 1 h.

For the production of Ag nanotriangles, 1 mL of $AgNO_3$ solution (20 mM) and 2 mL of 0.1 M AA were sequentially added into 40 mL of CTAB (10 mM). Then, 400 μL of the prepared seed solution were added into the above mixture. Finally, 400 μL of NaOH (1 M) were quickly added and the resulting solution was stirred for 10 min. A deep blue color appeared, signifying the formation of triangular Ag NPs. The synthesized NPs were centrifuged (8000 rpm, 10 min) and stored in the dark for characterization and applications.

2.3 Characterization

Ultraviolet–visible–near infrared (UV-vis-NIR) absorption spectroscopy measurements were recorded with a UV-vis spectrophotometer (UV-1900 (SHIMADZU)). The particle morphology was depicted using a Transmission Electron Microscope (TEM, JEOL JEM-2100Plus) and a Scanning Electron Microscope (SEM, ZEISS Sigma 300).

2.4 Simulations

The computational domain in the COMSOL simulation is a cubical volume with each side measuring 350 nm, which is enveloped by a 50 nm-thick perfectly matched layer (PML). The incident field is precisely constrained to a power of 1 watt, with its polarization vector oriented along the *y*-axis. The amplitude of the field is directly proportional to its power. As depicted in Fig. 8c, the silver nanosphere has a radius of 25 nm, and it is subjected to an incident field that propagates in the *x*-direction. Fig. 8d illustrates a different scenario where the incident field is directed along the *z*-axis, while the polariz-

ation remains aligned with the *y*-axis. The silver nanotriangle, featured in the simulation, boasts a side length of 52.7 nm and a thickness of 14 nm. Notably, all of its edges are rounded with a radius of 3 nm. The refractive index of silver was taken from the experiments of Johnson and Christy.[39] Throughout the simulation process, the silver nanostructures were placed in a vacuum environment.

2.5 Antimicrobial activity of silver NPs

The synthesized Ag nanospheres and Ag nanotriangles were tested for their antibacterial activity against the Gram-negative bacterium *Escherichia coli* (*E. coli*) and the Gram-positive bacterium *Staphylococcus aureus* (*S. aureus*).

2.5.1 Preparation of bacterial suspension. *E. coli* and *S. aureus* were cultured with sterilized LB liquid medium at 37 °C overnight, and then diluted to 1×10^8 colony forming unit (CFU) per mL with sterile normal saline (the OD_{600} (optical density at 600 nm wavelength) was about 0.1).

2.5.2 Zone of inhibition test. The antibacterial performance of Ag NPs was evaluated against *E. coli* and *S. aureus* using the agar well diffusion method[40] on LB agar medium. The test organisms were spread on separate LB agar medium plates, and wells of 8 mm diameter were constructed. AgNP suspension at a concentration of 120 μg mL^{-1} was filled in separate wells. The plates were incubated at 37 °C for 24 h. After the incubation period, the antibacterial activities were assessed by measuring the inhibition zone diameter.

2.5.3 Determination of the minimum inhibitory concentration (MIC) and minimum bactericidal concentration (MBC) of Ag NPs. The MIC of AgNPs was determined according to the method described by Naghizadeh and co-workers.[41] AgNPs were twofold serially diluted using sterile LB liquid medium in a 2 mL centrifuge tube. An equal amount of adjusted test microorganisms was added to each centrifuge tube. The tubes were incubated at 37 °C for 24 h. The MIC is defined as the lowest concentration of an antimicrobial agent to inhibit the visible growth of a microorganism after 24 h of incubation.

To evaluate the MBC of AgNPs, 100 μL samples were taken from all tubes without turbidity (from the MIC test) and they were transferred to LB liquid medium at 37 °C for 24 h. The MBC was determined as the lowest concentration of the sample in the tube corresponding to the agar plate without bacterial growth.[42] All tests were performed in triplicate for each sample.

2.5.4 Bacterial growth kinetics curve analysis. Bacterial suspensions were inoculated into LB liquid media containing Ag NPs in a range of different concentrations. The suspensions were co-cultured at 37 °C for 24 h, and the absorbance at 600 nm was measured at 0, 2, 4, 6, 8, 10, 12, and 24 h with a multi-microplate reader (VarioskanTM LUX, Thermo Fisher Scientific, Shanghai, China). Untreated bacterial culture served as the control. Growth curves were plotted based on the OD_{600} measurements.

2.5.5 Time-dependent killing curve analysis. The time-dependent killing experiments of *E. coli* and *S. aureus* in the presence of Ag NPs were carried out according to the method described by Pobiega *et al.*[43] The *E. coli* and *S. aureus* were inoculated into LB liquid medium containing Ag NPs at 1/2 MIC and MIC, respectively. The inoculations were incubated at 37 °C and aliquots were taken to perform colony count every 4 h for 24 h. The viable cells were determined by plating ten-fold serial dilutions for each sample at suitable time points and enumerating colonies after a 24 h incubation stage at 37 °C. The time-kill curves were drawn by plotting mean colony counts *versus* time.

2.5.6 Relative survival rate analysis. The relative survival rates of *E. coli* and *S. aureus* were calculated following the method described by Shen *et al.*[44] Bacterial suspensions were mixed with Ag NPs and co-cultured on a shaker at 37 °C for 4 h. Next, the collected bacteria were diluted 105-fold with normal saline, and 100 μL of bacterial suspension were spread on LB nutrition agar plates. After being incubated at 37 °C for 24 h, the colony population of bacteria was counted to evaluate the antibacterial ability of Ag NPs. The relative survival rate of bacteria was calculated using the following formula:

$$\text{Relative survival rate} = \frac{CFU_t}{CFU_0} \times 100\%$$

where CFU_0 denotes the number of colonies in the control group and CFU_t signifies the number of colonies in the AgNP groups.

2.5.7 Morphological changes of bacteria. The morphological alterations of bacteria treated with Ag NPs were determined by SEM. Bacterial suspensions were treated with Ag NPs at the MIC and sterile saline (control), respectively, at 37 °C for 4 h. After incubation, cells were collected by centrifugation at 8000 rpm for 10 min, washed with PBS buffer, and then incubated with 2.5% glutaraldehyde overnight at 4 °C. Following washing with PBS, the samples were hydrated with ascending concentrations of ethanol (30%, 50%, 70, 90%, 100%) with different ratios of hydrated : *tert*-butanol (2 : 1, 1 : 1). Then the samples were dried through freeze-drying. Finally, the dried samples were fixed on a SEM support and sputter-coated with gold under vacuum for SEM observation (Hitachi Regulus 8100, Tokyo, Japan).

2.5.8 Detection of reactive oxygen species (ROS). A ROS assay kit based on dihydroethidium (DHE) was used to measure the amount of ROS produced by bacteria. The bacteria were treated with different concentrations of AgNPs at 37 °C for 4 h. Afterwards the bacteria cells were washed with Tris-HCl buffer (10 mM, pH = 7.4), and 10 μM DHE was added. The bacteria were then incubated in the dark or under light at 37 °C. Untreated bacterial culture acted as a negative control. The fluorescence intensity (excitation/emission wavelength: 518 nm/610 nm) was recorded at 0, 30, 60, 90 and 120 minutes, and a kinetic curve was plotted.

2.6 Statistical analysis

All tests were conducted in triplicate. Data were expressed as mean ± SD values. Statistical analysis using one-way ANOVA analysis was followed by Duncan's test for posterior analysis using SPSS software.

3. Results and discussion

The synthetic strategy followed to obtain Ag nanotriangles was based on our previous work, using a seed-mediated growth route.[38] As shown in Fig. 1a, the TEM image reveals triangle-like nanoparticles with an edge length of *ca.* 42 nm. The morphologies of Ag nanotriangles are depicted in Fig. 1a and b, illustrating triangular configurations in the presence of tips. The concentration of Ag nanotriangle dispersions is about 120 μg mL^{-1}, estimated by the total conversion yields of silver precursors. HRTEM imaging of Ag nanotriangles helped to study their crystallinity profiles, revealing their {111} facets (Fig. 1c). In Fig. 1d (black line), there are two typical SPR peaks in the visible region at 548 nm and 411 nm corresponding to dipolar in-plane resonance. Meanwhile, there is another LSPR peak at 340 nm in the UV region assigned to the multipolar out-of-plane resonance. In contrast, the as-prepared Ag nanospheres appear indeed to exhibit a sphere-like shape, as observed in the SEM images (Fig. S1a†). Only a unique LSPR peak can be spotted at 405 nm in the visible range due to the isotropic particle morphology (Fig. S1b†).

In order to investigate the antibacterial performance of Ag NPs with different morphologies against *E. coli* and *S. aureus*, the main operating parameters, namely the antibacterial zone diameters, MBC/MIC ratio, growth curves and antibacterial curves, were screened. The antibacterial zone diameters were calculated by measuring the transparent circle formed around the pore, revealing the antibacterial effect of Ag NPs. In this work, we identified that the antibacterial zone diameters of Ag nanotriangles (120 μg mL^{-1}) against *E. coli* and *S. aureus* were 9 ± 0 mm and 19.67 ± 0.29 mm, respectively. However, Ag nanospheres with the same concentration did not show any obvious antibacterial zone diameter, due to the tip effect of Ag NPs (shown in Table S1†).

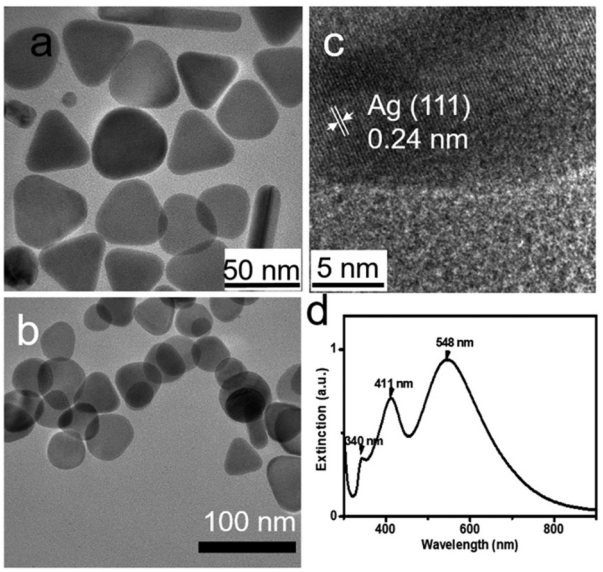

Fig. 1 (a and b) TEM images of Ag nanotriangles with different magnifications. (c) HRTEM image of Ag nanotriangles. (d) UV-vis-NIR spectrum of Ag nanotriangles.

The MBC/MIC ratio is a common parameter used for the evaluation of the bactericidal performance of antimicrobial agents. More specifically, antimicrobial agents are considered as bactericidal agents when the MBC/MIC ratio is between 1 and 2. On the other hand, the drug is considered a bacteriostatic agent when the MBC/MIC ratio is ≥4. As shown in Table S2,† under normal conditions, the MIC values of Ag NPs were 60 μg mL^{-1} while the MBC values were greater than 60 μg mL^{-1} for either *E. coli* or *S. aureus*, respectively. This indicates that the required antibacterial concentration for Ag nanospheres is relatively high, and the MBC/MIC ratio cannot be determined under these conditions. However, the MBC/MIC ratio of Ag nanotriangles is 2 for either *E. coli* or *S. aureus*, correspondingly. This illustrates that silver nanotriangles can be employed as bactericidal agents.

Furthermore, the growth curves of the bacteria were monitored according to the modifications of OD_{600} values in the UV-Vis spectra, shedding light on the bacterial growth kinetics; this was quantified by taking into account the absorbance of bacterial culture density. The effects of different concentrations of Ag nanospheres and Ag nanotriangles on the growth of *E. coli* and *S. aureus* are shown in Fig. S2 and S3.† It can be clearly noticed that the growth curves slow down as the concentration of Ag NPs increased, for both Ag nanospheres and Ag nanotriangles. The growth curve is inhibited by the oxidative stress response, due to the damage of bacterial cells *via* the tip effects of Ag NPs. Besides, as the concentration of NPs increased, the inhibition difference between Ag nanospheres and Ag nanotriangles became significant. In particular, Ag NPs with a concentration of 60 μg mL^{-1} totally prevented the growth of *E. coli* and *S. aureus*. Afterwards, the growth kinetics of the bacteria was examined in the presence of Ag NPs with a concentration of MIC, 1/2 MIC and 1/4 MIC (the MIC of Ag nanospheres was 60 μg mL^{-1} for both *E. coli* and *S. aureus*, while the MIC of Ag nanotriangles was 0.47 μg mL^{-1} for *E. coli* and 0.24 μg mL^{-1} for *S. aureus*.), see Fig. 2. In the control group, the OD_{600} value of *E. coli* and *S. aureus* gradually increased with time, while the OD_{600} value was kept constant at the MIC. Thus, Ag NPs at the MIC are sufficient to hinder the growth of *E. coli* and *S. aureus*. As shown in Fig. 2a and c, Ag nanospheres at 1/4 MIC (15 μg mL^{-1}) did not display almost any inhibitory effect. In contrast, the OD_{600} values of *E. coli* and *S. aureus* in Fig. 2b and d increased very slowly, implying that the inhibitory effect of Ag nanotriangles at 1/4 MIC (*E. coli*: 0.12 μg mL^{-1}; *S. aureus*: 0.006 μg mL^{-1}) is stronger in comparison to that of Ag nanospheres. In summary, Ag nanospheres and Ag nanotriangles affect the growth curves of *E. coli* and *S. aureus*, and as the concentration of Ag NPs increases, the greater the inhibitory effect on the bacteria, which shows a concentration-dependent trend (Fig. 3).[45]

Moreover, the antibacterial activity of Ag NPs as a function of their morphology and dosage was studied against Gram-negative *E. coli* and Gram-positive *S. aureus*. Although both types of Ag NPs display an antibacterial effect, the death speed

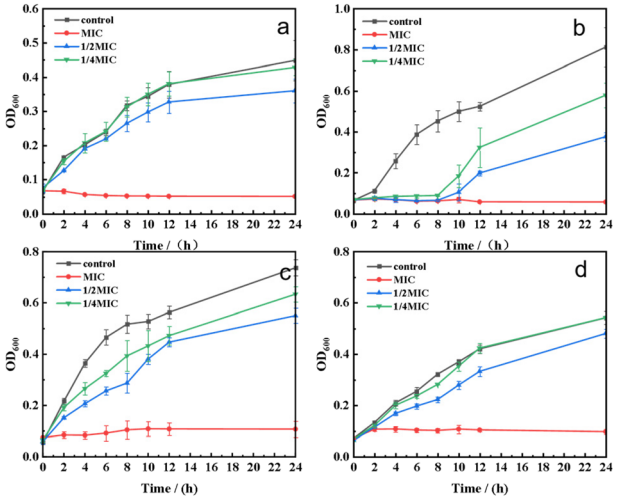

Fig. 2 The inhibitory effect of Ag NPs on the growth kinetics of bacteria. The growth kinetics of *E. coli* in the presence of Ag nanotriangles (a) and Ag nanospheres (c) were monitored by the alterations of OD_{600} values. The growth kinetics of *S.* aureus in the presence of Ag nanotriangles (b) and Ag nanospheres (d) were evaluated by considering the changes of OD_{600} values. Note: The MIC of Ag nanospheres was 60 μg mL^{-1} for both *E. coli* (c) and *S. aureus* (d), and the MIC of Ag nanotriangles was 0.47 μg mL^{-1} for *E. coli* (a) and 0.24 μg mL^{-1} for *S. aureus* (b).

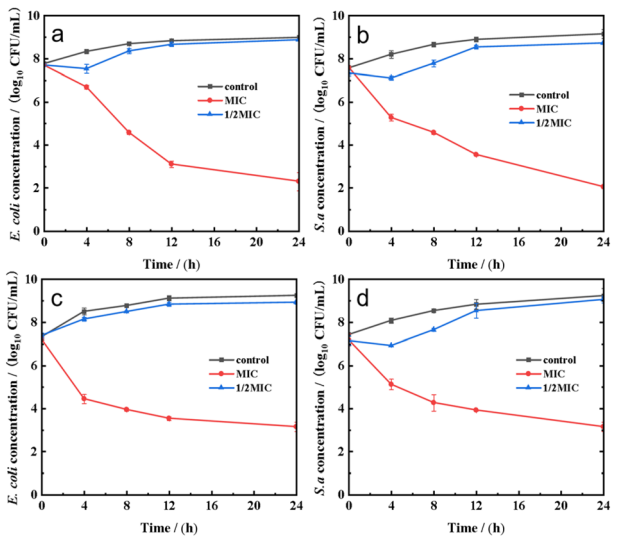

Fig. 3 The bactericidal kinetics of *E. coli* in the presence of Ag nanospheres (a) and Ag nanotriangles (c) were monitored by recording the alterations of OD_{600} values. The bactericidal kinetics of *S.* aureus in the presence of Ag nanospheres (b) and Ag nanotriangles (d) were examined by considering the modifications of OD_{600} values. Note: The MIC of Ag nanospheres was 60 μg mL^{-1} for both *E. coli* (a) and *S. aureus* (c), while the MIC of Ag nanotriangles was 0.47 μg mL^{-1} for *E. coli* (b) and 0.24 μg mL^{-1} for *S. aureus* (d).

of Gram-positive bacteria was faster than that of Gram-negative bacteria in the presence of Ag NPs attributed to their different bacterial membrane structures. In Fig. S4,† the antibacterial performance of Ag nanospheres and Ag nanotriangles at different concentrations is demonstrated, revealing a strong dose-dependent relationship.[46] As the concentrations of the two types of silver nanostructures increased, the growth of both *E. coli* and *S. aureus* decreased. In addition, the antibacterial activity of Ag nanotriangles was higher compared to that of Ag nanospheres. Even when assessing Ag nanotriangles with a quite low concentration, they still exhibited good antibacterial activity against both types of bacteria tested. The excellent antibacterial activity of Ag nanotriangles is mainly attributed to their tip effect, which enables the release of more Ag ions and the bacterial membrane can be penetrated in a more facile manner.

To further investigate the antibacterial mechanism of Ag NPs, the overall morphologies of the cells were monitored with SEM, depicting the changes in the cell membrane structure. A whole, robust cell can serve as a protective barrier for the cell itself while a broken cell membrane shall lead to cell damage. The cellular contents would leak out, provoking ultimately cell death. Therefore, investigating the changes in the cell membrane morphology is a critical means to evaluate and better understand the inhibitory effects of antibacterial agents on bacteria.[48] In addition, the broken cell membrane will inhibit their growth. As observed in the SEM images in Fig. 4a, *E. coli* and *S. aureus*, which were not treated with Ag NPs or light, feature a whole rod-like and sphere-like shape enclosed with a smooth and rounded surface, respectively. Once treated with Ag NPs, the bacterial morphologies were modified: in particular, *E. coli* cells showed cracks, wrinkles, fractures and leakage

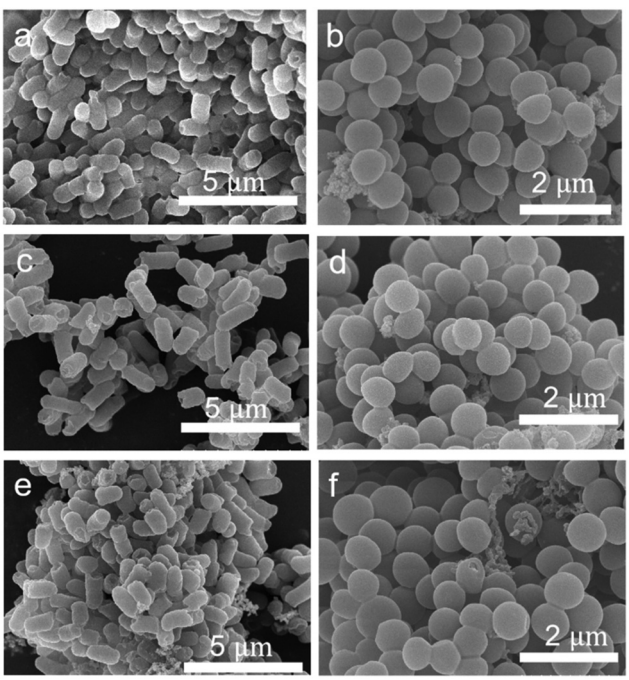

Fig. 4 SEM images of untreated *E. coli* (a) and *S. aureus* (b) (no Ag NPs or sunlight irradiation used). Under non-illumination conditions: SEM images of *E. coli* (c) and *S. aureus* (d) treated with Ag nanospheres; SEM images of *E. coli* (e) and *S. aureus* (f) treated with Ag nanotriangles.

of contents, whereas the *S. aureus* cells shrank and developed surface holes.

Under light irradiation, Ag displays a stronger localized surface plasmon resonance (LSPR) property in comparison to Au and Cu. LSPR will be irradiated into the electromagnetic field and hot electrons which are applied in the fields of surface-enhanced spectroscopy, cancer therapy and photocatalysis. Concerning antibacterial performance, the environmental oxygen gets oxidized by the hot electrons to superoxide (*e.g.* $^1O_2$), which is the main contributor to the antibacterial activity. LSPR of metal NPs strongly depends on their size, composition and morphology; therefore the generation efficiency of $^1O_2$ relies on the particle morphologies to a significant extent. In this manuscript, we have utilized Ag nanostructures with sphere-like and triangular shapes as antibacterial agents. Under the irradiation of sunlight at noon for 0.5 h, the MIC of Ag nanospheres was 60 μg mL^{-1} against both *E. coli* and *S. aureus* while its MBC was also 60 μg mL^{-1} against these bacteria, respectively. Under the same conditions, the MIC and MBC of Ag nanotriangles against *E. coli* were both 0.47 μg mL^{-1}, while the MIC and MBC of Ag nanotriangles against *S. aureus* were both 0.24 μg mL^{-1}. Under sunlight irradiation, the MBC/MIC ratio for both Ag nanospheres and Ag nanotriangles is equal to 1, whereas such a ratio in the case of Ag nanotriangles is 2 under normal conditions (no sunlight). This indicates the enhancement of the antibacterial activity of Ag NPs by applying sunlight irradiation.

Under light irradiation, Ag NPs not only exhibited typical concentration-dependent antibacterial activity but also showed the LSPR effect. After being exposed to sunlight, the growth curves of Ag NPs on *E. coli* and *S. aureus* are shown in Fig. S6.† The Ag NPs displayed good antibacterial properties against both types of bacteria after light exposure, especially at 1/4 MIC (the 1/4 MIC of Ag nanospheres was 15 μg mL^{-1} for both *E. coli* and *S. aureus*, while the 1/4 MIC of Ag nanotriangles was 0.012 μg mL^{-1} for *E. coli* and 0.006 μg mL^{-1} for *S. aureus*.) The OD_{600} of *E. coli* and *S. aureus* treated with Ag nanospheres and Ag nanotriangles was consistently lower than that of the control group, indicating significant inhibition of bacterial growth. In particular, the OD_{600} value was almost kept at zero when treated with Ag NPs at the MIC, indicating the effect of light on the antibacterial performance of Ag NPs (the MIC of Ag nanospheres was 60 μg mL^{-1} for both *E. coli* and *S. aureus*, and the MIC of Ag nanotriangles was 0.47 μg mL^{-1} for *E. coli* and 0.24 μg mL^{-1} for *S. aureus*.) To further investigate the antibacterial behavior of Ag NPs, the viable cell populations of bacteria were counted in the dark and under light irradiation, respectively. In Fig. S6,† the viable cell populations of bacteria in the control group increased with the incubation time within 24 h. However, at the MIC, the viable cell counts of both bacteria treated with Ag nanospheres and Ag nanotriangles significantly decreased in comparison to the control group, indicating their distinct antibacterial activity. For the viable cell counts of bacteria treated with Ag NPs for 8 h, there were only inhibitory effects observed, while the bacterial populations were not completely killed. In contrast, after 0.5 h of light irradiation, the bactericidal curves of Ag NPs applied to treat the bacteria are shown in Fig. S7,† revealing no viable cells at their MIC. At the same MIC of Ag NPs without light irradiation, there are inhibitory effects and limited bacterial killing. Light will promote the inhibitory effects and bacterial killing properties of Ag NPs due to their LSPR properties. At 1/2 MIC concentration, the LSPR properties of Ag nanotriangles boost their antibacterial activity within 12 h (the 1/2 MIC of Ag nanospheres was 30 μg mL^{-1} for both *E. coli* and *S. aureus*, whereas the 1/2 MIC of Ag nanotriangles was 0.24 μg mL^{-1} for *E. coli* and 0.12 μg mL^{-1} for *S. aureus*).

As shown in Fig. S8,† the survival rates of *E. coli* and *S. aureus* under light conditions in the absence of Ag NPs were 94.0% and 93.5%, respectively. Sunlight has a certain bactericidal effect, but this effect is not significant. After further treatment with 7.5 μg mL^{-1}, 15 μg mL^{-1} and 30 μg mL^{-1} Ag nanospheres without sunlight irradiation for 4 hours, the relative survival rates of *E. coli* decreased to 95%, 84.5%, and 57.9%, respectively. However, after sunlight irradiation for 0.5 h, the survival rates decreased to 81.3%, 42.1%, and 28.9%, respectively (Fig. S8a and b†). At a concentration of 60 μg mL^{-1}, no live bacteria were observed, with a survival rate of 0%. Similarly, *S. aureus* showed the same trend after Ag nanosphere treatment, implying that sunlight can enhance the antibacterial effects of silver nanoparticles (Fig. S8c and d†). After being treated with Ag nanotriangles, both *E. coli* and *S. aureus* showed no viable cell counts and exhibited strong antibacterial properties even at very low concentrations (Fig. 5). As one can see from the SEM images in Fig. 6a and b, *E. coli* and *S. aureus* untreated with Ag NPs but treated with sunlight for 0.5 h are depicted: the rod-like shapes of *E. coli* are broken to a small degree, while the sphere-like structures of *S. aureus* are almost kept intact. Once the bacteria are treated with both Ag NPs and sunlight, their morphologies become significantly broken (Fig. 6c–f). The *E. coli* aggregate and break when treated with both types of Ag NPs. Nevertheless, it is clearly shown that the damage degree of the bacteria treated with Ag nanotriangles is

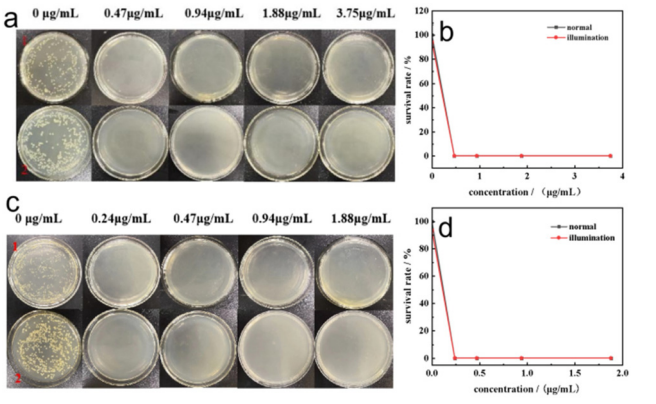

Fig. 5 The photographs of *E. coli* (a) and *S. aureus* (c) treated with different amounts of Ag nanotriangles and their corresponding survival rates (b) and (d), respectively (sunlight).

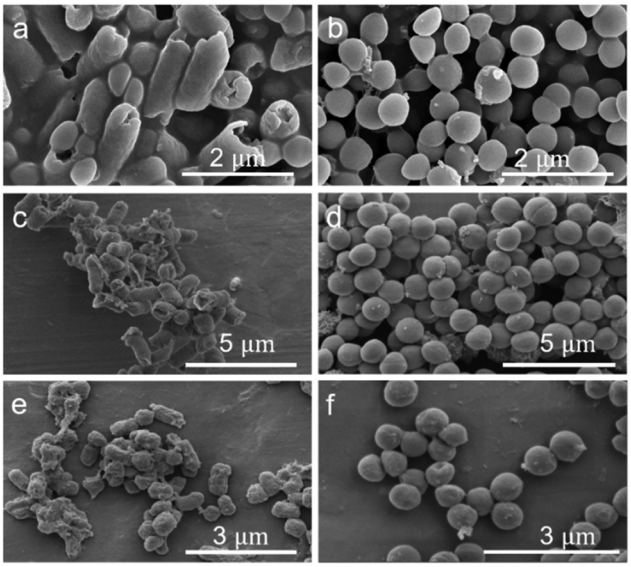

Fig. 6 SEM images of *E. coli* (a) and *S. aureus* (b) without Ag NP treatment, but treated with sunlight. Under sunlight irradiation conditions: SEM images of *E. coli* (c) and *S. aureus* (d) treated with Ag nanospheres; SEM images of *E. coli* (e) and *S. aureus* (f) treated with Ag nanotriangles.

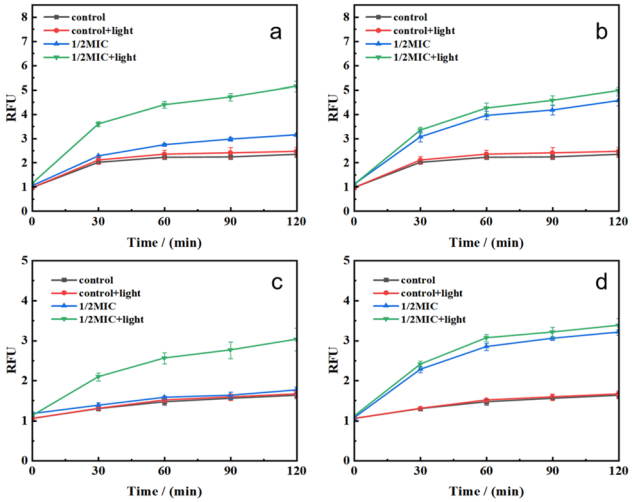

Fig. 7 ROS generation curves of *E. coli* treated with Ag nanotriangles (a) and Ag nanospheres (b). ROS generation curves of *S. aureus* treated with Ag nanotriangles (c) and Ag nanospheres (d). The concentration of Ag NPs is 1/2 MIC. Note: The 1/2 MIC of Ag nanospheres was 30 μg mL^{-1} for both *E. coli* (a) and *S. aureus* (c), while the 1/2 MIC of Ag nanotriangles was 0.24 μg mL^{-1} for *E. coli* (b) and 0.12 μg mL^{-1} for *S. aureus* (d).

larger than that treated with Ag nanospheres under sunlight irradiation.

Oxidative stress is a normal physiological response of cells. However, when oxidative stress exceeds the capacity of the cell to handle it, it can cause damage to the cell. The level of oxidative stress is closely related to the level of ROS in microorganisms.[47] The production of ROS is considered to be the main pathway for the antimicrobial effect of Ag NPs, in particular in the presence of light irradiation. In this manuscript, the fluorescent probe dihydroethidium (DHE) was used to quantitatively detect the generation efficiency of reactive oxygen species (ROS). DHE can freely enter cells through the cell membrane and is oxidized by ROS inside the cells to form oxidized ethidium. The oxidized ethidium can intercalate into chromosomal DNA, resulting in the observation of new red fluorescence. Thus, the quantities of ROS can be evaluated by measuring the intensities of the new red fluorescence. In Fig. 7 and S9,† the quantities of ROS in bacteria treated with both Ag NPs and light irradiation were the highest in comparison to the other 'partially treated' samples. When the bacteria were treated with the same concentration of Ag NPs, the generation rate of ROS increased with the irradiation time (Fig. 7). In addition, the generation rate of ROS when bacteria were treated with Ag nanotriangles was higher than in the case of treatment with Ag nanospheres under light irradiation.

Therefore, two mechanisms for the antibacterial function in the presence of Ag NPs are proposed in this manuscript. In Fig. 8a, Ag NPs can interact with cell membranes and release silver ions to react with proteins, causing oxidative damage to microbial cells. The bacterial death is triggered by the release of Ag ions from Ag NPs on the cell membrane. It is also observed that bacterial morphologies are damaged when treated with both types of Ag NPs. Nonetheless, under sunlight irradiation, LSPR of Ag NPs will be irradiated into the hot electrons, participating in the generation of strong oxidation agents (*i.e.*, hydroxyl radicals, hydrogen peroxide, superoxide anions, singlet oxygen ($^1O_2$)) (Fig. 8b). These ROS can oxidatively damage biomolecules such as lipids, proteins and nucleic acids, effectively killing microorganisms.[49] In addition, the LSPR of nanoparticles is strongly dependent on their morphologies. From Fig. 8c and d, the tips on the Ag nanotriangles will attract high densities of hot electrons; thus the Ag

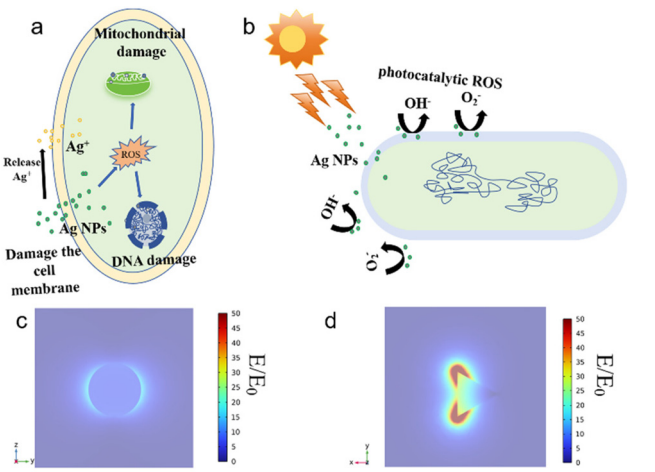

Fig. 8 (a) The antibacterial mechanism of Ag NPs towards the tested bacteria under dark conditions; (b) the antibacterial mechanism of Ag NPs under sunlight irradiation; (c and d) the simulated electromagnetic field around the Ag nanospheres and nanotriangles.

nanotriangles show a higher intensity of near-field distribution. This situation will provide abundant sources for the generation of singlet oxygen ($^1O_2$).

4. Conclusions

In this study, two types of Ag NPs (nanospheres and nanotriangles) exhibited antibacterial activity against Gram-positive and Gram-negative bacteria. Previous studies reported that the thicker layer of peptidoglycan on the Gram-positive bacteria *S. aureus* can protect against the disruption of Ag^+ and Ag NPs on the cell membranes. It has also been reported that the thinner lipopolysaccharide layer of the Gram-negative bacteria *E. coli* makes them more sensitive to Ag antibacterial agents. However, in the present work, the Gram-positive bacteria *S. aureus* were shown to be more sensitive to Ag NPs. In other words, Ag NPs displayed better antibacterial activity against *S. aureus* than against *E. coli*. This may be due to the stronger interaction between lipopolysaccharide in Gram-negative bacteria and Ag NPs compared to the cell wall of Gram-positive bacteria, and lipopolysaccharide may block the positively charged Ag^+ coming from Ag NPs. Therefore, a higher amount of Ag NPs and Ag^+ will be needed to kill bacteria of *E. coli* type. In addition, the antibacterial performance of Ag NPs was shown to be highly dependent on their morphologies. Ag nanotriangles displayed a better antibacterial effect than Ag nanospheres against both bacterial types irrespective of the presence of light irradiation; this was ascribed to their tip effect and LSPR properties.

Author contributions

All of the authors have contributed to the writing of the manuscript.

Data availability

The data that support the findings of this study will be available on reasonable request from the corresponding author.

Conflicts of interest

There are no conflicts to declare.

Acknowledgements

This work was supported by the National Natural Science Foundation of China (Grants No. 32202063, 22271257, 21902148), the Natural Science Foundation of Henan (Grant No. 232300421096) and the Doctoral Fund of Henan University of Technology (2021BS053). S. G. G. acknowledges support by the project CNS2022-135531 (funded by MICIU/AEI/10.13039/501100011033 and European Union Next Generation EU/PRTR).

References

1 X. Zhang, D. Liu, T. Z. Jin, W. Chen and M. Guo, Preparation and characterization of gellan gum-chitosan polyelectrolyte complex films with the incorporation of thyme essential oil nanoemulsion, *Food Hydrocolloids*, 2020, **114**, 106570.
2 S. Tripathi, L. Kumar, R. K. Deshmukh and K. K. Gaikwad, Ultraviolet blocking films for food packaging applications, *Food Bioprocess Technol.*, 2024, **17**, 1563–1582.
3 S. Ahmed, D. E. Sameen, R. Lu, R. Li, J. Dai, W. Qin and Y. Liu, Research progress on antimicrobial materials for food packaging, *Crit. Rev. Food Sci. Nutr.*, 2022, **62**, 3088–3102.
4 X. Liu, L. Ji, X. Wang, J. Li, J. Zhu and A. Sun, Role of Rpos in stress resistance, quorum sensing and spoilage potential of Pseudomonas fluorescens, *Int. J. Food Microbiol.*, 2018, **270**, 31–38.
5 S. Karanth, S. Feng, D. Patra and A. K. Pradhan, Linking microbial contamination to food spoilage and food waste: the role of smart packaging, spoilage risk assessments and date labeling, *Front. Microbiol.*, 2023, **14**, 1198124.
6 H. S. James and M. S. Segovia, Behavioral ethics and the incidence of foodborne illness outbreaks, *J. Agric. Environ. Ethics*, 2020, **33**, 531–548.
7 N. A. Al-Tayyar, A. M. Youssef and R. Al-Hindi, Antimicrobial food packaging based on sustainable bio-based materials for reducing foodborne pathogens: A review, *Food Chem.*, 2020, **310**, 125915.
8 L. Ye, Z. Cao, X. Liu, Z. Cui, Z. Li, Y. Liang, S. Zhu and S. Wu, Noble metal-based nanomaterials as antibacterial agents, *J. Alloys Compd.*, 2022, **904**, 164091.
9 M. Abbas, M. Ovais, A. Atiq, T. M. Ansari, R. Xing, E. Spruijt and X. Yan, Tailoring supramolecular short peptide nanomaterials for antibacterial applications, *Coord. Chem. Rev.*, 2022, **460**, 214481.
10 Y. W. Zhao, J. Xie, Y. Z. Tian, S. Mourdikoudis, N. Fiuza-Maneiro, Y. L. Du, L. Polavarapu and G. C. Zheng, Colloidal chiral carbon dots: an emerging system for chiroptical applications, *Adv. Sci.*, 2024, **11**, 2305797.
11 J. Chen, X. Liu, G. Zheng, W. Feng, P. Wang, J. Gao, J. Liu, M. Wang and Q. Wang, Detection of glucose based on noble metal nanozymes: mechanism, activity regulation and enantioselective recognition, *Small*, 2023, **19**, 2205924.
12 M. Xu, Y. Song, J. Wang and N. Li, Anisotropic transition metal-based nanomaterials for biomedical applications, *View*, 2021, **2**, 20200154.
13 X. Li, Z. Tan, B. Guo, C. Yu, M. Yao, L. Liang, X. Wu, Z. Zhao, F. Yao, H. Zhang, S. Lyu, C. Yuan and J. Li, Magnet-oriented hydrogels with mechanical-electrical anisotropy and photothermal antibacterial properties for

wound repair and monitoring, *Chem. Eng. J.*, 2023, **463**, 142387.
14 X. Liu, Y. Du, S. Mourdikoudis, G. Zheng and K. Y. Wong, Chiral magnetic oxide nanomaterials: Magnetism meets chirality, *Adv. Opt. Mater.*, 2023, **11**, 2202859.
15 B. Le Ouay and F. Stellacci, Antibacterial activity of silver nanoparticles: A surface science insight, *Nano Today*, 2015, **10**, 339–354.
16 X. Li, G. Gao, C. Sun, Y. Zhu, L. Qu, F. Jiang and H. Ding, Preparation and antibacterial performance testing of Ag nanoparticles embedded biological materials, *Appl. Surf. Sci.*, 2015, **330**, 237–244.
17 Z. Guo, Y. Chen, Y. Wang, H. Jiang and X. Wang, Advances and challenges in metallic nanomaterial synthesis and antibacterial applications, *J. Mater. Chem. B*, 2020, **8**, 4764–4777.
18 Z. M. Xiu, Q. B. Zhang, H. L. Puppala, V. L. Colvin and P. J. J. Alvarez, Negligible particle-specific antibacterial activity of silver nanoparticles, *Nano Lett.*, 2012, **12**, 4271–4275.
19 W. R. Li, T. L. Sun, S. L. Zhou, Y. K. Ma, Q. S. Shi, X. B. Xie and X. M. Huang, A comparative analysis of antibacterial activity, dynamics and effects of silver ions and silver nanoparticles against four bacterial strains, *Int. Biodeterior. Biodegrad.*, 2017, **123**, 304–310.
20 G. A. Sotiriou and S. E. Pratsinis, Antibacterial activity of nanosilver ions and particles, *Environ. Sci. Technol.*, 2010, **44**, 5649–5654.
21 P. Pallavicini, A. Taglietti, G. Dacarro, Y. Antonio Diaz-Fernandez, M. Galli, P. Grisoli, M. Patrini, G. Santucci De Magistris and R. Zanoni, Self-assembled monolayers of silver nanoparticles firmly grafted on glass surfaces: Low Ag^+ release for an efficient antibacterial activity, *J. Colloid Interface Sci.*, 2010, **350**, 110–116.
22 A. Balestri, J. Cardellini and D. Berti, Gold and silver nanoparticles as tools to combat multidrug-resistant properties, *Curr. Opin. Colloid Interface Sci.*, 2023, **66**, 101710.
23 X. Hou, H. Ma, F. Liu, J. Deng, Y. Ai, X. Zhao, D. Mao, D. Li and B. Liao, Synthesis of Ag ion-implanted TiO_2 thin films for antibacterial application and photocatalytic performance, *J. Hazard. Mater.*, 2015, **299**, 59–66.
24 X. Bi, Q. Bai, M. Liang, D. Yang, S. Li, L. Wang, J. Liu, W. W. Yu, N. Sui and Z. Zhu, Silver peroxide nanoparticles for combined antibacterial sonodynamic and photothermal therapy, *Small*, 2022, **18**, 2104160.
25 R. T. P. da Silva, M. V. Petri, E. Y. Valencia, P. H. C. Camargo, S. I. C. de Torresi and B. Spira, Visible light plasmon excitation of silver nanoparticles against antibiotic-resistant Pseudomonas aeruginosa, *Photodiagn. Photodyn. Ther.*, 2020, **31**, 101908.
26 S. Wang, X. Liu, S. Mourdikoudis, J. Chen, W. Fu, Z. Sofer, Y. Zhang, S. Zhang and G. Zheng, Chiral Au nanorods: Synthesis, chirality origin and applications, *ACS Nano*, 2022, **16**, 19789–19809.
27 G. Zheng, S. Mourdikoudis and Z. Zhang, Plasmonic metallic heteromeric nanostructures, *Small*, 2020, **16**, 2002588.
28 B. Ouyang, D. Wei, B. Wu, L. Yan, H. Gang, Y. Cao, P. Chen, T. Zhang and H. Wang, In the view of electrons transfer and energy conversion: The antimicrobial activity and cytotoxicity of metal-based nanomaterials and their applications, *Small*, 2024, **20**, 2303153.
29 Z. Zhu, H. Luo, T. Wang, C. Zhang, M. Liang, D. Yang, M. Liu, W. W. Yu, Q. Bai, L. Wang and N. Sui, Plasmon-exchanged peroxidase-like activity of nitrogen-doped graphdiyne oxide quantum dots/gold-silver nanocage heterostructures for antimicrobial applications, *Chem. Mater.*, 2022, **34**, 1356–1368.
30 Z. Liu, Z. Chen, H. Xie, Y. Cui, H. J. Feng and K. Hua, The effect of electron transfer channel on UV-independent antibacterial activity of Ag^+ implanted TiO_2, *Appl. Surf. Sci.*, 2023, **624**, 157147.
31 A. Hezam, N. Abutaha, F. A. Almekhlafi, A. M. Nagi Saeed, P. Abishad and M. A. Wadaan, Smart plasmonic Ag/Ag_2O/ZnO nanocomposite with promising photothermal and photodynamic antibacterial activity under 600 nm visible light illumination, *J. Photochem. Photobiol., A*, 2023, **435**, 114322.
32 S. Jiang, C. Cui, W. Bai, W. Wang, E. Ren, H. Xiao, M. Zhou, C. Cheng and R. Guo, Shape-controlled silver nanoparticles colored fabric with tunable colors, photothermal antibacterial and colorimetric detection of hydrogen sulfide, *J. Colloid Interface Sci.*, 2022, **626**, 1051–1061.
33 K. Chávez, Y. Salinas-Delgado, L. A. Bretado, M. A. Gómez-Hurtado, I. Santos-Ramos, R. Pérez and G. Rosas, Synthesis of silver flower-like particles and evaluation of their antibacterial activity, *Mater. Lett.*, 2024, **357**, 135774.
34 S. Tang and J. Zheng, Antibacterial activity of silver nanoparticles: Structural effects, *Adv. Healthcare Mater.*, 2018, **7**, 1701503.
35 M. R. El-Zahry, A. Mahmoud, I. H. Refaat, H. A. Mohamed, H. Bohlmann and B. Lendl, Antibacterial effect of various shapes of silver nanoparticles monitored by SERS, *Talanta*, 2015, **138**, 183–189.
36 P. Ray, T. Lodha, A. Biswas, T. K. Sau and C. V. Ramana, Particle specific physical and chemical effects on antibacterial activities: A comparative study involving gold nanostars, nanorods and nanospheres, *Colloids Surf., A*, 2021, **634**, 127915.
37 T. Guo, S. H. Zhuang, H. L. Qiu, Y. T. Guo, L. L. Wang, G. X. Jin, W. W. Lin, G. M. Huang and H. H. Yang, Black phosphorus nanosheets for killing bacteria through Nanoknife effect, *Part. Part. Syst. Charact.*, 2020, **37**, 2000169.
38 S. L. Jiao, Y. X. Liu, S. L. Wang, S. Wang, F. Y. Ma, H. Y. Yuan, H. B. Zhou, G. C. Zheng, Y. Zhang, K. Dai and C. T. Liu, Face-to-face assembly of Ag nanoplates on filter papers for pesticide detection by surface-enhanced Raman spectroscopy, *Nanomaterials*, 2022, **12**, 1398.
39 P. B. Johnson and R. W. Christy, Optical Constants of the Noble Metals, *Phys. Rev. B: Solid State*, 1972, **6**, 4370.
40 S. Nayaka, M. P. Bhat, B. Chakraborty, S. S. Pallavi, D. Airodagi, R. Muthuraj, H. M. Halaswamy,

S. B. Dhanyakumara, K. N. Shashiraj and C. Kupaneshi, Seed Extract-mediated synthesis of silver nanoparticles from Putranjiva roxburghii Wall., phytochemical characterization, antibacterial activity and anticancer activity against MCF-7 cell line, *Indian J. Pharm. Sci.*, 2020, **82**, 260–269.

41 S. Mortazavi-Derazkola, M. Hosseinzadeh, A. Yousefinia and A. Naghizadeh, Green synthesis and investigation of antibacterial activity of silver nanoparticles using Eryngium bungei Boiss plant extract, *J. Polym. Environ.*, 2021, **29**, 2978–2985.

42 M. Bhat, B. Chakraborty, R. S. Kumar, A. I. Almansour, N. Arumugam, D. Kotresha, S. S. Pallavi, S. B. Dhanyakumara, K. N. Shashiraj and S. Nayaka, Biogenic synthesis, characterization and antimicrobial activity of Ixora brachypoda (DC) leaf extract mediated silver nanoparticles, *J. King Saud Univ., Sci.*, 2020, **33**, 101296.

43 K. Pobiega, K. Krasniewska, J. L. Przybyl, K. Baczek, J. Zubernik, D. Witrowa-Rajchert and M. Gniewosz, Growth biocontrol of foodborne pathogens and spoilage microorganisms of food by Polish Propolis Extracts, *Molecules*, 2019, **24**, 2965.

44 C. Q. Shen, Y. M. Xue, Y. X. Li, M. Wei, M. Y. Wei, M. Y. Wen, L. B. Zhang and L. Shang, Kinetically regulated one-pot synthesis of cationic gold nanoparticles and their size-dependent antibacterial mechanism, *J. Mater. Sci. Technol.*, 2023, **162**, 145–156.

45 S. M. Navarro Gallón, E. Alpaslan, M. Wang, P. Larese-Casanova, M. E. Londoño, L. Atehortúa, J. J. Pavon and T. J. Webster, Characterization and study of the antibacterial mechanisms of silver nanoparticles prepared with microalgal exopolysaccharides, *Mater. Sci. Eng., C*, 2019, **99**, 685–695.

46 C. L. D. Dicastillo, M. G. Correa, F. B. Martínez, C. Streitt and M. J. Galotto, Antimicrobial effect of titanium dioxide nanoparticles, in *Antimicrobial Resistance-A One Health Perspective*, IntechOpen, 2020. DOI: **10.5772/INTECHOPEN.90891**.

47 C. Z. Chen and S. L. Cooper, *Biomaterials*, 2002, **23**, 3359–3368.

48 A. Salleh, R. Naomi, N. D. Utami, A. W. Mohammad, E. Mahmoudi, N. Mustafa and M. B. Fauzi, The potential of silver nanoparticles for antiviral and antibacterial applications: a mechanism of action, *Nanomaterials*, 2020, **10**, 1566.

49 R. Yin, T. H. Dai, P. Avci, A. E. S. Jorge, W. C. M. A. de Melo, D. Vecchio, Y. Y. Huang, A. Gupta and M. R. Hamblin, Light based anti-infectives: ultraviolet C irradiation, photodynamic therapy, blue light and beyond, *Curr. Opin. Pharmacol.*, 2013, **13**, 731–762.